Experiments on Adaptive Antenna Array Diversity Receiver/Transmitter for W-CDMA BTS Application

Hidekazu Taoka, Taisuke Ihara, Kenichi Higuchi, and Mamoru Sawahashi

Wireless Laboratories, NTT DoCoMo, Inc.
3-5 Hikari-no-oka, Yokosuka-shi, Kanagawa, 239-8536 Japan
E-mail: taoka@mlab.yrp.nttdocomo.co.jp

Abstract - This paper presents experimental results on the coherent adaptive antenna array diversity (CAAAD) receiver and adaptive antenna array transmit diversity (AAA-TD) for application to W-CDMA base transceiver station (BTS), in order to increase further the radio link capacity in the reverse and forward links assuming a frequency division duplex (FDD) system. In our scheme, the transmitter antenna weights in AAA-TD are generated from the receiver antenna weights in the CAAAD receiver by performing two calibrations: carrier frequency calibration and RF circuitry calibration. Successive laboratory experiments using multipath fading simulators and phase shifters elucidate the profound interference suppression effect of the CAAAD receiver and AAA-TD coupled with orthogonal variable spreading factor (OVSF) code usage in the reverse and forward links, respectively. Furthermore, field experimental results elucidate that the required transmission power at the average block error rate (BLER) of 10^{-2} employing the CAAAD receiver with four antennas is reduced above 2 dB compared to that using four-antenna space diversity reception when the ratio of the target signal energy per bit-to-interference plus background noise power spectrum density ratio (E_b/I_0) of the desired user to interfering user for fast transmission power control (TPC) is $\Delta E_b/I_0$ = - 15 dB, and that even when the transmitted signal-to-interference power ratio (SIR) is -12 dB, no error floor is observed with AAA-TD and the loss of the required received signal power at the average bit error rate (BER) of 10^{-3} from the single-user case is suppressed to below approximately 5 dB.

I. Introduction

Associated with the successive introduction planning of commercial Wideband-Code Division Multiple Access (W-CDMA) [1] services from 2001 on a global scale, the genuine era of wireless Internet is dawning. In W-CDMA, all users communicate simultaneously in the same frequency band and consequently, multiple access interference (MAI) is the major cause of transmission impairment in the reverse link. Employing an adaptive antenna array receiver is a promising technique to reduce the severe MAI [2]-[7]. Meanwhile, in IMT-2000, the amount of traffic in the forward link is expected to be much greater than that in the reverse link since high-speed data download services through the Internet and broadcast services etc. will be provided in the near future. In the forward link, although orthogonality among the channels that travel through the same propagation path is achieved using orthogonal variable spreading factor (OVSF) [8] codes, each channel suffers from severe multipath interference (MPI) especially from high rate users, who transmit at high power. Following the above-mentioned background of the requirements, we proposed the coherent adaptive antenna array diversity (CAAAD) in the reverse link and adaptive antenna array transmit diversity (AAA-TD) [5]-[7] in the forward link based on the W-CDMA air interface [8], [9]. In the AAA-TD scheme, transmitter antenna weights were generated by modifying the receiver antenna weights generated in the CAAAD receiver [3]-[4], which is a practical scheme for adaptive antenna array receivers [2]. However, since frequency division duplex (FDD) is used in W-CDMA systems, the instantaneous phase and amplitude variations due to fading in the reverse link have no correlation to those in the forward link. In our CAAAD design, the adaptive antenna array forms a receiver beam pattern that tracks only changes in the directions of arrival (DOAs) of the desired and interfering users, and the Rake combiner tracks the instantaneous variations in the channel conditions to maximize instantaneous signal-to-interference plus background noise power ratio (SINR).

In the forward link, the transmitter beam pattern, in which the maximum gain is generated toward the direction of the desired signal. Therefore, in AAA-TD, the transmitter antenna weights are generated by performing two calibrations, i.e., RF circuitry calibration and carrier frequency calibration to the corresponding receiver antenna weights generated in the CAAAD receiver[8]-[9].

This paper presents experimental results on the CAAAD receiver and AAA-TD for application to W-CDMA base transceiver station (BTS), in order to increase further the radio link capacity in the reverse and forward links. In the paper, the overall configuration of the adaptive antenna array diversity transceiver and the receiver antenna weight generation method are first described in the following section. Then, we presents the motivation and principles of carrier frequency calibration and RF circuitry calibration to generate transmitter antenna weights in the forward link. Finally, the laboratory and field experimental results are analyzed.

2. CAAAD and AAA-TD Configuration

2.1 Overall Configuration

The overall block diagram of the BTS transceiver including the CAAAD receiver in the reverse link and AAA-TD in the forward link is given in Fig. 1. In the reverse link, after down-conversion and linear amplification by an automatic gain control (AGC) amplifier, the received spread signal at each antenna is converted into baseband in-phase (I) and quadrature (Q) components by a quadrature detector. The I and Q signals are sampled at *n* times the chip rate (where the integer value of *n* denotes the over-sampling factor). After filtration using a square-root raised cosine Nyquist filter, the sampled data sequences are fed into the CAAAD processing block. The receiver antenna weights for each user are adaptively generated in the CAAAD processing block. The antenna weight-combined function and coherent Rake combining employing pilot channel-based channel estimation are also included in the CAAAD block. The Rake-combined data sequence is channel-decoded to recover the transmitted data sequence.

In our scheme, the transmitter antenna weights in the forward link are generated based on the receiver antenna weights by performing two calibrations: carrier frequency calibration and RF circuitry calibration. The channel-encoded data sequence is multiplied by the transmitter antenna weights and spread using the combination of a cell-specific scrambling code and OVSF code. After filtering, spreading data sequences are converted into an analog format and then quadrature-modulated into an IF or RF signal followed by power-amplification.

2.2 Receiver Antenna Weight Generation Method

A block diagram of the CAAAD processing block based on the minimum mean squared error (MMSE) criterion is illustrated in Fig. 2. The CAAAD block comprises digital matched filters (MFs), a digital beam former, a pilot symbol-assisted (PSA)-coherent Rake combiner, and an antenna weight controller. The sequence of the filtered received signal samples is first despread by the MFs and then resolved into each path component that are propagated along different propagation paths. The resolved path is multiplied by the receiver antenna weight and combined. This process is valid when the fading correlation among antennas is almost 1 assuming high-elevation antennas and a short antenna separation such as $\lambda/2$ (λ is the carrier wave length). The receiver antenna weight, i.e., the receiver beam pattern, is common to all paths for Rake combin-

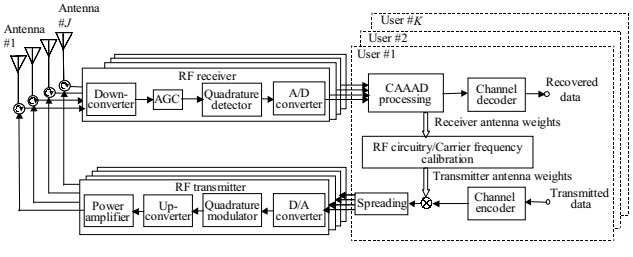

Fig. 1. Overall block diagram of adaptive antenna array transceiver.

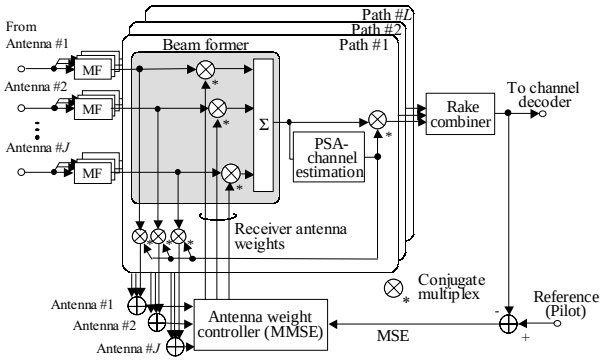

Fig. 2 Block diagram of CAAAD receiver

ing. The complex channel gain of each resolved path after antenna weight combining is estimated using pilot symbols multiplexed into the Q-channel. The paths for Rake combining are searched based on the block-averaged power delay profile. The receiver antenna weights are adaptively controlled so that the mean squared error (MSE) between the Rake combined signal and the reference signal is minimized using an adaptive algorithm such as the RLS (Recursive Least Squares) or N-LMS (normalized least mean square) algorithms [11]. Details on the antenna-updating algorithm are given in [3]. The pilot symbols multiplexed into the Q-channel and tentative decision data symbols, i.e., binary-decided data sequence before/after channel decoding, are used as a reference signal.

3. Calibration for Transmitter Antenna Weights

3.1 Carrier Frequency Calibration

As described in Section 1, our concern is the FDD system, which employs different carrier frequencies in the reverse and forward links, nevertheless using the common array antennas with the antenna separation of half the carrier wavelength in the reverse link (λ_{RX}). When the receiver antenna weights are directly used as transmitter antenna weights, the generated transmitter beam pattern is shifted from the receiver beam pattern since the difference in the propagation distance between antennas differs due to the different carrier frequencies. Let θ be the azimuth angle of the incoming signal in the reverse link. Then, the phase difference corresponding to the difference in the propagating distance, A ($= \lambda_{RX} \sin\theta/2$), between two adjacent antennas in the reverse link, δ, becomes

$$\delta = A \times \frac{2\pi}{\lambda_{RX}} = \pi \sin\theta \quad . \tag{1}$$

In the CAAAD processing block, receiver antenna weights are generated to compensate for the phase difference. The difference in the propagating distance, B, when the receiver antenna weights are applied directly in the forward link, is expressed as

$$B = \delta \times \frac{\lambda_{TX}}{2\pi} = \frac{\lambda_{TX}}{2} \sin\theta \quad . \tag{2}$$

where λ_{TX} is the carrier wave length in the forward link. Let θ' be the direction of the main lobe in the generated transmitter beam pattern. Then, since B is identical to $\lambda_{RX} \sin\theta'/2$, θ' is derived as

$$\theta' = \sin^{-1}\left(\frac{\lambda_{TX}}{\lambda_{RX}} \sin\theta\right) = \sin^{-1}\left(\frac{f_{RX}}{f_{TX}} \sin\theta\right) \quad . \tag{3}$$

Clearly from (3), the direction of the main lobe in transmitter beam pattern θ' is shifted from the correct azimuth of incoming signal θ except for the case when $\theta = 0$. Thus, carrier frequency calibration is required to generate the transmitter antenna weights[7]. In the paper, we shift the direction of the main lobe in the transmitter beam pattern so that it coincides with the main lobe in the receiver beam pattern. One example of the generated beam pattern with/without carrier frequency calibration is shown in Fig. 3. We first obtain the direction θ having the highest antenna gain in the receiver beam pattern. The angle difference between the reverse and forward links in the directions yielding the maximum antenna gain in the beam pattern due to the carrier frequency difference, $\Delta\theta$, is expressed as

$$\Delta\theta = \sin^{-1}\left\{\left(\frac{f_{TX}}{f_{RX}} - 1\right)\sin\theta\right\} \quad . \tag{4}$$

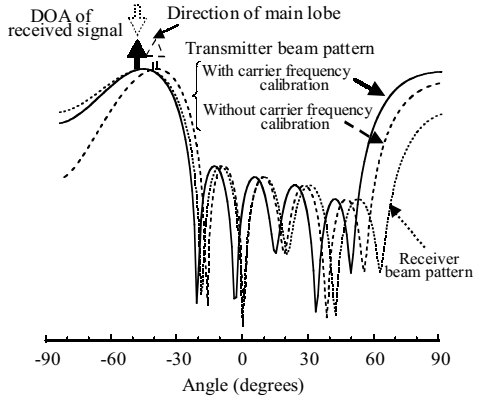

Fig.3 Carrier frequency calibration for generating transmitter antenna weights in FDD

The transmitter antenna weights are generated by rotating the receiver antenna weight by $\Delta\theta$, where $R(\Delta\theta)$ is a steering vector expressed as

$$R(\Delta\theta) = (1, e^{j\pi\sin\Delta\theta}, e^{j2\pi\sin\Delta\theta}, e^{j3\pi\sin\Delta\theta}, \ldots) \quad . \tag{5}$$

In the packet mode, where there are fewer DSCHs(Downlink Shared Channels) than the degrees of freedom of array antenna, the carrier frequency calibration toward the directions of the bean nulls in addition to that toward the main lobe is beneficial for decreasing multipath interference from other DSCHs with large transmission power.

3.2 RF Circuitry Calibration

Fig. 1 clearly shows that the receiver antenna weights generated in the CAAAD receiver are influenced by the transfer function (phase/amplitude variation) of the parallel RF receiver circuitry and that the transmitted signals are influenced by the transfer function of the parallel RF transmitter circuitry. These transfer functions of the RF receiver/transmitter are different due to the active components. Thus, in the CAAAD receiver, the generated receiver antenna weights of each antenna are reflected in the transfer function of the RF receiver circuitry as well as the incoming signal conditions at the antennas. To obtain the receiver antenna weights that reflect only the incoming signal conditions, the effect of the transfer function of the RF receiver circuitry must be eliminated. This is done by

$$w_P^{(j)} = w_{RX}^{(j)} \cdot x_{RX}^{(j)} \quad . \tag{6}$$

where $w_P^{(j)}$, $w_{RX}^{(j)}$, and $x_{RX}^{(j)}$ are the ideal complex-valued receiver antenna weight that reflects only the incoming signal conditions, the generated complex-valued receiver weight in the CAAAD receiver, and the complex-valued transfer function of the RF receiver circuitry of the j-th antenna, respectively. The weights in (6) cannot be directly applied for transmission because the weighted signal at the baseband signal processing suffers from phase/amplitude shift due to the RF transmitter circuitry. Therefore, the transfer function of the RF transmitter circuitry is compensated for at the baseband transmitter beam forming processing stage. When $x_{TX}^{(j)}$ is the transfer function of the RF transmitter circuitry of the j-th antenna, the transmitter weight, $w_{TX}^{(j)}$, at the baseband beam forming stage can be obtained from

$$w_{TX}^{(j)} = w_P^{(j)} \cdot x_{TX}^{(j)-1} = w_{RX}^{(j)} \cdot (x_{RX}^{(j)} \cdot x_{TX}^{(j)-1}) \quad . \tag{7}$$

By calibrating the RF receiver/transmitter to the generated receiver antenna weights in the CAAAD receiver block, the maximum gain is obtained toward the direction of the desired signal. The transmitter antenna weight for the j-th antenna after both RF circuitry calibration and carrier frequency calibration is represented as

$$w_{TX}^{(j)} = w_{RX}^{(j)} \cdot R^{(j)}(\Delta\theta) \cdot (x_{RX}^{(j)} \cdot x_{TX}^{(j)-1}) \quad . \tag{8}$$

where $R^{(j)}(\Delta\theta)$ is the j-th element of $R(\Delta\theta)$.

4. Laboratory Experiments

The major radio link parameters of the implemented base station transceiver are listed in Table 1. In the laboratory experiments, fading simulators were used to generate multipath signals that follow independent 2-path Rayleigh fading with the maximum Dop-

Table1. Major radio link parameters

		Reverse		Forward
Chip rate (Bandwidth)		4.096 Mchip/s (5 MHz)		
Carrier frequency		1,990.5 MHz		2,175 MHz
Frame structure		I/Q-Mux pilot channel		Time-Mux pilot channel
Symbol rate		I	64 ksps	64 ksps
		Q	16 ksps	
Information bit rate		18.9 kbps		29.6 kbps
Spreading factor (SF)		I	64	64
		Q	256	
Spreading	Channelization code	Walsh-Hadamard sequences		
	Scrambling code	Truncated-Gold sequence		
		40,960 chips		40,960 chips
Modulation	Data	BPSK		QPSK
	Spreading	QPSK		
Channel estimation		Pilot symbol-assisted channel estimation		
		3-slot averaging		4-slot averaging
Channel coding and decoding		Convolutional coding (R = 1/3, K = 9) Soft-decision Viterbi decoding		
Interleaving size		20 ms		

pler frequency, f_D. The delay time difference between paths was set to 1.0 μs. We assumed a linear array with the separation of $\lambda_{RX}/2$. The fading simulator output was divided into four, each of which was phase shifted and combined with other user signals, where the phase shift is given by $180\times(j-1)\sin\theta$ degrees for the j-th antenna, where θ is the arrival angle. In the experiments, we set the angle spread of +/-5 degrees between the two paths. Finally, Gaussian noise was added to obtain the composite received spread signal at each antenna element and was input into the receiver. SINR-based closed-loop transmission power control (TPC) [12] was used as the fast TPC.

First, the measured average bit error rate (BER) performance employing the CAAAD receiver with four antennas with fast TPC is plotted in Fig.4 as a function of the average transmitted signal energy per bit-to-background noise power ratio (E_b/N_0) in two-user environment (one-interfering user). The parameter on the horizontal axis varies by changing the target signal energy per bit-to-interference plus background noise power spectrum density ratio (E_b/I_0) value in fast TPC. The ratio of the target E_b/I_0 for fast TPC of the desired user to interfering user is a parameter. Thus, when $\Delta E_b/I_0$ = -12 dB, the average received E_b/I_0 after Rake combining of the interfering user is 12 dB greater than that of the desired user. We assume that f_D is 5 Hz. The BER performance without fast TPC is also shown in the figure for comparison. We find from the figure that when fast TPC is not employed, the average BER performance employing the CAAAD receiver is degraded compared to that with space diversity (SD) reception with maximal ratio combining (MRC) thanks to the diversity effect except for the case with $\Delta E_b/I_0$ = -12 dB. However, we find that when the fast TPC is used, the achievable BER performance with the CAAAD receiver is almost identical to that with the SD receiver for the $\Delta E_b/I_0$ of greater than -6 dB. Furthermore, we find that the required transmit E_b/N_0 at the average BER of 10^{-3} with the CAAAD receiver is reduced by approximately 1.5 dB compared to that with the SD receiver for the $\Delta E_b/I_0$ of -12 dB. These results indicate that the BER degradation caused by the drops in the received signal due to fading is complementarily mitigated by fast TPC.

Next, The measured average BER performance of a desired user using AAA-TD with four antennas both with RF circuitry calibration and carrier frequency calibration is plotted in Fig. 5 as a function of the average transmit E_b/N_0 in a four-user environment (three interfering users). Transmit E_b/N_0 of AAA-TD indicates the average transmitted signal energy per bit of all four antennas-to-background noise power ratio. The DOAs of the desired and interfering users were set to θ_D = -50 degrees and θ_U = -20, +15, +45 degrees, respectively. The BER performance is shown for when $\Delta E_b/I_0$, was -3, -5, and -12 dB and that for one-user case (i.e., no interfering user) is also shown for comparison. Clearly, in the one-user case, the decrease in the required transmit E_b/N_0 of approximately 5.4 dB with AAA-TD from that with one antenna transmitter corresponds to the increased antenna gain. Figure 5 shows that as $\Delta E_b/I_0$ is decreased, the BER performance with the 1 antenna transmitter is severely degraded and an error floor is observed due to the remarkably increasing MPI from the interfering users. Especially, when $\Delta E_b/I_0$ is -12 dB, the obtained BER is almost 10^{-1}. However, the figure shows the significant interference suppression effect of AAA-TD, i.e., almost the same BER performance as that obtained in the one-user case, is achieved when the average transmit E_b/N_0 is lower than 5 dB for $\Delta E_b/I_0$ = -3 dB, -5 dB, and even -12 dB. When $\Delta E_b/I_0$ = -3 and -5 dB, the required average transmit E_b/N_0 at the average BER of 10^{-3} with four-antennas AAA-TD was decreased by approximately 7.5 and 18 dB compared to that with the one antenna transmitter, because of the interference suppression effect through beam steering in addition to the increased antenna gain.

5. Field Experiments

Field experiments were conducted in an area nearby Tokyo in a two-user environment (hereafter we denote the desired and interfering users as mobile station(MS)#1 and MS#2, respectively). The antenna heights of the base station and the mobile stations were 50 and 2.9 meters from the ground, respectively. We measured the beam pattern and BER performance when MS#1 equipped with a mobile transceiver was driven along the measurement courses at an average speed of approximately 30 km/h and MS#2 was stationary at a fixed location. In the measurement course, the look angle of MS#1 from the base station was changed from +40 degrees to +60 degrees and MS#2 was stationary at the look angle of -25 degrees. A residential apartment building and an office building were located along the measurement course. So a power delay profile with one-to-two path was observed, while MS#2 was almost in the line-of-sight path (thus, a single path).

First, the time variation performance of the generated receiver beam pattern of MS#1 during a 4500-frame interval (= 45 seconds) is depicted in Fig. 6. The target E_b/I_0 values of MS#1 and MS#2 in fast TPC were set to 9 dB and 21 dB, respectively. We see clearly from figures that the direction of the main lobe is precisely changed according to the change of the DOA of the MS#1 and that the null or lower-gain receiver beam is generated toward the direction of MS#2. The measured average block error rate (BLER) performance employing the CAAAD receiver and SD reception with MRC using 4 antennas is plotted in Fig. 7 as a function of the relative transmission power of MS#1. Block length was 20 ms. Fig. 7 shows the BLER performance when the ratio of the target E_b/I_0 of

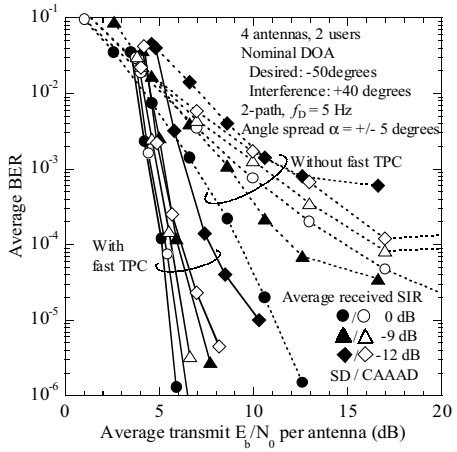

Fig. 4 Average BER performance of CAAAD receiver as function of average transmit E_b/N_0 per antenna (Laboratory experiment)

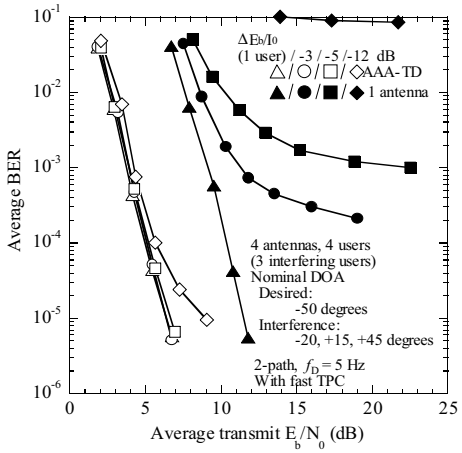

Fig. 5 Average BER performance with AAA-TD as function of average transmit E_b/N_0 (Laboratory experiment)

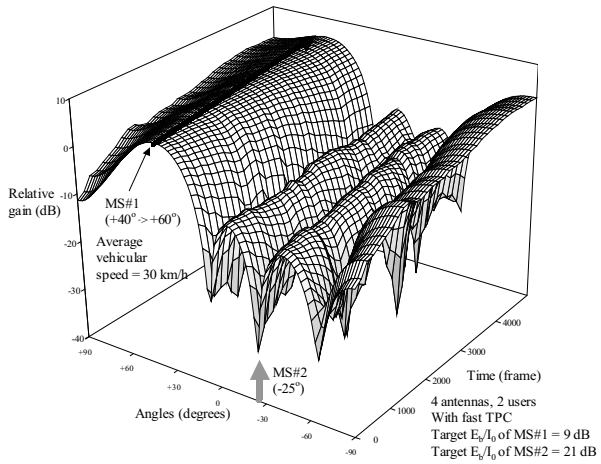

Fig. 6 Receiver beam pattern in field experiment

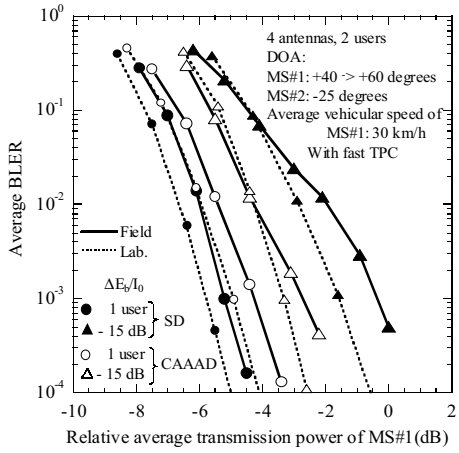

Fig. 7 Average BLER performance as a function of average transmission power in reverse link (Field experiments)

MS#1 to that of MS#2 was $\Delta E_b/I_0$ = -12 and -15 dB, respectively. The laboratory experimental results assuming the two-path model with f_D = 80 Hz and with the angle spread between two paths of +/- 5 degrees are also plotted as dotted lines in the figure. The transmission power of MS#1 was normalized by that satisfying the average BLER of 10^{-2} with single-antenna reception in a single-user environment. We find from the figure that the required transmission power at the average BLER of 10^{-2} attained in the field experiments is increased by approximately 0.5-1.0 dB compared to that in the laboratory experiments. This is because the propagation channel model in the laboratory experiments is not accurately identical to that in the filed experiments, and path search error occurs especially for a path with lower received power of Rake combining due to the decrease of received signal power per antenna. Nevertheless, we can find that the decrease in the transmission power employing the CAAAD receiver from that using the SD reception in the field experiments is almost the same as that in the laboratory experiments when $\Delta E_b/I_0$ = -15 dB. The required transmission power using the SD reception is significantly increased when $\Delta E_b/I_0$ = -15 dB, however, that employing the CAAAD receiver is kept slightly lower owing to the strong interference suppression effect of the CAAAD receiver. The figure shows that the required transmission power at the average BLER of 10^{-2} employing the CAAAD receiver is reduced above 2 dB compared to that using the SD reception with the identical number of antennas when $\Delta E_b/I_0$ = -15 dB and that the loss in the required transmission power of the CAAAD receiver in the same situation from that in single-user environment is approximately 1 dB.

Finally, the measured average BER performance employing four-antenna AAA-TD is plotted in Fig. 8 as a function of the average received signal power of MS#1 with the average transmitted SIR before multiplying the transmitter antenna weights as a parameter. The reverse link average received E_b/N_0 for MS#1 was set to 25

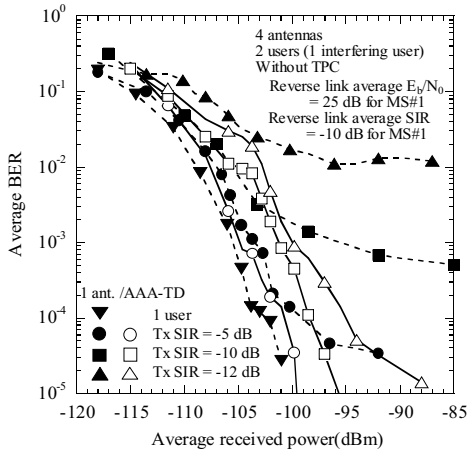

Fig. 8 Average BER performance as a function of received signal power in forward link (Field experiments)

dB. It was assumed that the average received SIRs at a BS in the reverse link for MS#1 was -10 dB. For comparison, the results with a one-antenna transmitter are also plotted. The figure shows the error floors due to the severe MPI are observed for the one-antenna transmitter, especially when the average transmitted SIR is low. However, the BER with AAA-TD is significantly improved due to the interference suppression effect. Even when the transmitted SIR is -12 dB, no error floor is observed with AAA-TD and the loss of the required received signal power at the average BER of 10^{-3} from the single-user case is suppressed to below approximately 5 dB.

6. Conclusion

This paper presented experimental results on the CAAAD receiver and AAA-TD for application to a W-CDMA BTS, in order to increase further the radio link capacity in the reverse and forward links assuming an FDD system. In our scheme, the transmitter antenna weights in AAA-TD are generated from the receiver antenna weights in the CAAAD receiver by performing two calibrations: carrier frequency calibration and RF circuitry calibration. Successive laboratory experiments using multipath fading simulators and phase shifters elucidate the profound interference suppression effect of the CAAAD receiver and AAA-TD coupled with OVSF code usage in the reverse and forward links, respectively. Furthermore, field experimental results clarified that that the required transmission power at the average BLER of 10^{-2} employing the CAAAD receiver with four antennas is reduced above 2 dB compared to that using-four antena SD reception when $\Delta E_b/I_0$ in the SIR-based fast TPC was -15 dB and that even when the transmitted SIR is -12 dB, no error floor was observed with AAA-TD and the loss of the required received signal power at the average BER of 10^{-3} from the single-user case was suppressed to below approximately 5 dB.

References

[1] F. Adachi, M. Sawahashi, and H. Suda, "Wideband DS-CDMA for next generation mobile communications system," IEEE Commun. Mag., vol. 36, pp. 56-69, Sept. 1998.
[2] R.T. Compton, Jr., "An adaptive antenna in a spread-spectrum communication system," Proc. IEEE, vol. 66, pp. 289-295, March 1978.
[3] S. Tanaka, M. Sawahashi, and F. Adachi, "Pilot symbol-assisted decision-directed coherent adaptive array diversity for DS-CDMA mobile radio reverse link," IEICE Trans. Fundamentals, vol. E80-A, pp. 2445-2454, Dec 1997.
[4] S. Tanaka, A. Harada, and M. Sawahashi, "Experiments on coherent adaptive antenna array diversity for wideband DS-CDMA mobile radio," IEEE J. Select. Areas Commun., vol. 18, pp. 1495-1504, Aug. 2000.
[5] A. Harada, S. Tanaka, M. Sawahashi, and F. Adachi, "Performance of adaptive antenna array diversity transmitter for W-CDMA forward link," IEEE PIMRC'99, pp. 1134-1138, Osaka, Sept. 12-15, 1999.
[6] A. Harada, S. Tanaka, M. Sawahashi, and F. Adachi, "Experiments on adaptive antenna array transmit diversity in W-CDMA forward link," Proc. 5th CDMA International Conference (CIC), Vol. 2, pp. 47-51, Nov. 2000.
[7] H. Taoka, S. Tanaka, T. Ihara, and M. Sawahashi, "Experiments on adaptive antenna array transmit diversity with carrier frequency calibration in transmit power-controlled forward link for W-CDMA mobile radio," Proc. 3G Wireless'01, pp.555-560, May 2001.
[8] K. Okawa and F. Adachi, "Orthogonal forward link using orthogonal multi-spreading factor codes for coherent DS-CDMA mobile radio," IEICE Trans. Commun., Vol. E81-B, pp. 777-784, April 1998.
[9] 3GPP, 3G TS25.211, "Physical channels and mapping of transport channels onto physical channels (FDD)".
[10] 3GPP, 3G TR25.848, "Physical layer aspect of UTRA High Speed Downlink Packet Access".
[11] S. Haykin, *Adaptive Filter Theory*, Prentice Hall, NJ, 1991.
[12] S. Seo, T. Dohi, and F. Adachi, "SIR-based transmit power control of reverse link for coherent DS-CDMA mobile radio," IEICE Trans. Commun., vol. E81-B, pp. 1508-1516, July 1998.